Graphical abstract

Enantioselective domino alkyl arylation of vinyl phosphonates by combining photoredox and nickel catalysis

Tingzhi Lin,[a] Guorong Li,[b,1] Qianqian Lu,[a,1] Chen Zhang,[b,1] Yan-En Wang,[c] Fei Xing,[a] Yundong Xu,[a] Kun Yang,[a] Dan Xiong,[a] Xiufang Xu,[*,b] Patrick J. Walsh[*,d] and Jianyou Mao[*,a]

[a]*Institute of Advanced Synthesis, School of Chemistry and Molecular Engineering, Nanjing Tech University, 30 South Puzhu Road, Nanjing 211816, China.*
[b]*Department of Chemistry, Key Laboratory of Advanced Energy Materials Chemistry (Ministry of Education), College of Chemistry, Nankai University, 94 Weijin Road, Tianjin 300071, China.*
[c]*College of Science, Hebei Agricultural University, Baoding 071000, China.*
[d]*Roy and Diana Vagelos Laboratories, Penn/Merck Laboratory for High-Throughput Experimentation, University of Pennsylvania, Department of Chemistry, 231 South 34th Street, Philadelphia, Pennsylvania 19104, United States.*

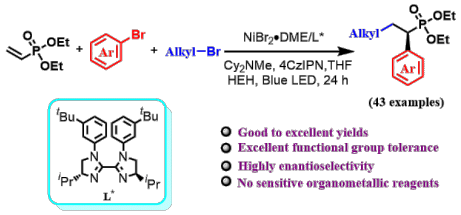

Herein, a three-component enantioselective cross-electrophile coupling protocol for nickel/photoredox complex mediated asymmetric alkyl arylations of vinyl phosphonates has been established. This dual catalytic protocol avoids using preformed organometallic reagents and brominated phosphorus derivatives, providing a diverse array of enantioenriched phosphonates with good to excellent yield and highly enantioselectivities.

Article

Enantioselective domino alkyl arylation of vinyl phosphonates by combining photoredox and nickel catalysis

Tingzhi Lin[a], Guorong Li[b,1], Qianqian Lu[a,1], Chen Zhang[b,1], Yan-En Wang[c], Fei Xing[a], Yundong Xu[a], Kun Yang[a], Dan Xiong[a], Xiufang Xu,[b,*] Patrick J. Walsh[d,*] and Jianyou Mao[a,*]

[a]*Institute of Advanced Synthesis, School of Chemistry and Molecular Engineering, Nanjing Tech University, 30 South Puzhu Road, Nanjing 211816, China.*
[b]*Department of Chemistry, Key Laboratory of Advanced Energy Materials Chemistry (Ministry of Education), College of Chemistry, Nankai University, 94 Weijin Road, Tianjin 300071, China.*
[c]*College of Science, Hebei Agricultural University, Baoding 071000, China.*
[d]*Roy and Diana Vagelos Laboratories, Penn/Merck Laboratory for High-Throughput Experimentation, University of Pennsylvania, Department of Chemistry, 231 South 34th Street, Philadelphia, Pennsylvania 19104, United States.*

ARTICLE INFO

Article history:
Received
Received in revised form
Accepted
Available online

Keywords:
three-component
enantioselective
nickel/visible light-catalyzed
reductive cross-coupling reactions
chiral *α*-aryl phosphonates

ABSTRACT

A nickel/photoredox mediated asymmetric domino alkyl arylation of vinyl phosphonates to generate a diverse array of enantioenriched *α*-aryl phosphonates is disclosed. This asymmetric three-component difunctionalization couples aryl halides and alkyl bromides with vinyl phosphonates, exhibiting excellent chemo- and regioselectivity under mild reaction conditions. The method avoids the need for pre-formed organometallics and phosphorus halides. Mechanistic and DFT studies suggest that photoexcited [4CzIPN]* oxidizes diethyl 1,4-dihydro-2,6-dimethyl-3,5-pyridinedicarboxylate (HEH) to generate the $[4CzIPN]^{\bullet-}$, which then reduces the alkyl bromide to form alkyl radicals that undergo Giese addition to the vinyl phosphonate. At the same time, Ni^0 oxidatively adds the aryl bromide followed by enantiodetermining oxidative radical trapping of the phosphonate-based radical by the tetrahedral Ni^{II} center followed by reductive elimination. Independent gradient model based on Hirshfeld partition (IGMH) analysis suggests that the orientation of the phosphonate group (P=O···π interaction) is expected to play an essential role in controlling the enantioselectivity.

1. Introduction

Phosphonates and their derivatives are important scaffolds with broad applications in medicinal chemistry [1-2], agrochemicals [3-4], and in applications as flame retardants and metal extractants [5]. They are also used as ligands in metal catalyzed processes, as redox catalysts [6] and are valuable precursors and reagents in organic synthesis (ex. Horner-Wadsworth-Emmons (HWE) and Arbuzov reactions) [7-9].

Enantioenriched phosphonates exhibit many desirable properties [5, 7-8, 10] and, therefore, their synthesis has attracted great interest. Only a few efficient enantioselective strategies, however, have been reported. For example, the asymmetric 1,4-conjugate addition of phosphorus-based nucleophiles to *α,β*-unsaturated carbonyls generates enantioenriched *β*-carbonyl phosphorus scaffolds [11-16]. Synthetic strategies involving direct asymmetric *α*-functionalization of organophosphorus compounds has emerged as an alternative to introducing chiral phosphonates [17-21]. Earlier routes to elaborate organophosphorus compounds include bromination followed by cross-coupling with classical nucleophiles [22-23]. In pioneering work, G. Fu and co-workers employed a Hiyama coupling of *α*-halo phosphonates to prepare racemic products (Scheme 1a) [22]. More recently, Y. Fu and Lu advanced an enantioselective nickel-catalyzed coupling of racemic *α*-brominated phosphonates by reductive hydroalkylation of olefins (Scheme 1b) [24]. To avoid pre-functionalization of organophosphorus reagents, we have demonstrated that *α*-P C–H deprotonative cross-coupling processes were effective for constructing racemic phosphonates (Scheme 1c) [25-26]. Unfortunately, the product C–H is more acidic than the starting phosphonate, rendering an enantioselective version based on this approach challenging.

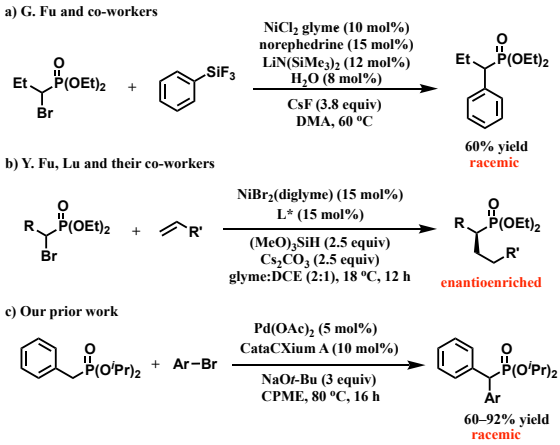

Scheme 1. Cross-coupling of existing organophosphorus.

Inspired by G. Fu and co-workers' pioneering asymmetric cross-coupling reactions [27-29], nickel-catalyzed

* Corresponding author.
E-mail address: *ias_jymao@njtech.edu.cn* (J. Mao) ; *xxfang@nankai.edu.cn* (X. Xu) ; *pwalsh@sas.upenn.edu* (P. J. Walsh)
[1]These authors contributed equally.

enantioselective reductive cross-couplings have attracted great interests. The advantage of reductive cross-couplings is that they circumvent the use of preformed organometallic reagents, which are moisture- and air-sensitive. Asymmetric reductive coupling methods mediated by stoichiometric metal reductants (zinc or manganese) have been advanced by the groups of Weix [30-32], Reisman [33-36], Doyle [37-39], Gong [40-41], Diao [42-43], Shu [44-46], Wang [47-51] and others [52-56]. To reduce the stoichiometric Zn and Mn waste, we reported a nickel/photoredox dual catalyst asymmetric cross-electrophile coupling of α-halo carbonyl compounds [57] using HEH (diethyl 1,4-dihydro-2,6-dimethyl-3,5-pyridinedicarboxylate) as reductant to make profen derivatives (Scheme 2a) [58]. This strategy was recently adopted by Xu and co-workers [59]. More recently, asymmetric nickel/photoredox dual catalyst cross-electrophile couplings have emerged as a valuable alternative to standard cross-couplings and have been further developed by Doyle [39, 60-61] and Xu [59, 62-66] as well as others (Scheme 2b and c) [62, 67]. It should be noted that during the preparation of this manuscript, Xu and co-workers published a 2-component nickel/photoredox catalyzed asymmetric coupling of α-bromophosphate and aryl iodides (Scheme 2d) [59].

In addition to the enantioconvergent two component cross-electrophile couplings (Scheme 2a–d), multicomponent reactions with olefins to afford diverse difunctionalized molecular skeletons have become a topic of interest [68]. Nevado and co-workers developed an asymmetric Ni-catalyzed tandem alkyl arylation of vinyl phosphonates by using TDAE as reductant, only one example was reported with 50% yield and 87% ee value (Scheme 2e) [69]. We previously realized the enantioselective domino alkyl arylation of acrylates. This method allowed efficient generation of a diverse array of nonsteroidal anti-inflammatory drug derivatives (NSAIDs) [57, 70-71]. Other researchers, including Chu [53-54, 72-73], Nevado [74], Martin [75] and Rueping [76-77] have introduced 3-component coupling reactions. These works inspired us to wonder if the nickel/photoredox approach could be applied to the asymmetric difunctionalization of vinyl phosphonates. Herein is presented an asymmetric tandem alkyl arylation of vinyl phosphonates to generate a diverse array of enantioenriched phosphonates with excellent chemo- and regioselectivity under mild reaction conditions (Scheme 2f). The method presented herein is complementary to the advances above and stands as a more straightforward approach to build complexity into phosphorus-based reagents.

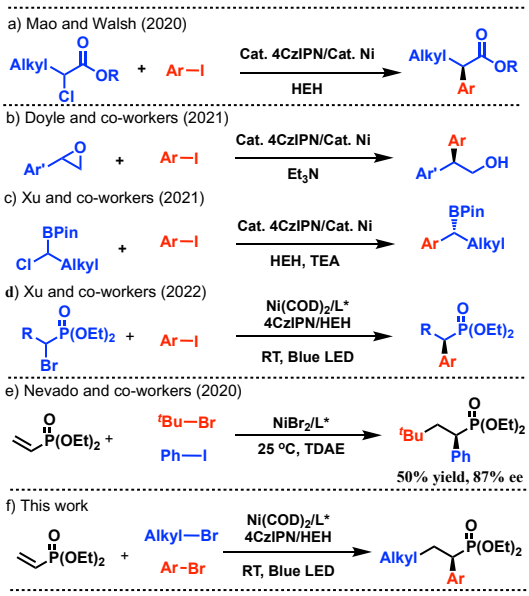

Scheme 2. Nickel/photoredox mediated asymmetric cross-coupling reactions.

2. Results and discussions

Based on our previous studies on nickel-catalyzed cross-electrophile coupling reactions [52, 55-57, 70, 78], we chose $Ni(COD)_2$/**L1*** as catalyst precursors. Diethyl vinylphosphonate **1a**, 1-(4-bromophenyl)ethan-1-one **2a** and 2-bromo-2-methylpropane **3a** were selected as model substrates. The reaction was carried out in dimethylacetamide (DMA) with HEH (reductant), Cy_2NMe base and catalytic 4CzIPN under irradiation with blue LED at room temperature for 24 h. The three-component cross-coupling product **4a** was generated with 95% ee and 25% assay yield (Table 1, entry 1) (assay yield = AY, determined by GC integration of the unpurified reaction mixture against an internal standard). We then tested a library of chiral ligands and found that **L1*** provided the highest ee value (see the Supporting Information table S1 for details). Next, a variety of nickel precursors were tested. $NiBr_2$·DME outperformed the other nickel sources [$Ni(COD)_2$, $NiBr_2$, NiI_2], providing the target product **4a** with 95% ee and 60% AY (Table 1, entry 4 *vs* entries 1–3). Next, alternative solvents were examined with $NiBr_2$·DME/**L1*** as the catalyst precursor. Tetrahydrofuran (THF) provided the desired product with 95% ee and 65% AY (Table 1, entry 7), exceeding others [DME (1,2-dimethoxyethane) and CPME (cyclopentyl methyl ether)] (Table 1, entries 5 and 6).

Further optimization of the reductant and concentration demonstrated that 2.0 equiv HEH with 0.05 mol/L THF improved the reaction AY to 75% with 95% ee (Table 1, entry 9). The loading of 4CzIPN was next varied and it was found that 2–5 mol% of 4CzIPN led to a slight decrease of the reaction efficiency (Table 1, entries 10 and 11), while 1 mol% 4CzIPN improved the AY to 88% (85% isolated yield) with 95% ee (Table 1, entry 12). We hypothesize that the intermediate [**L1***Ni^{II}(Br)Ar] concentration must be properly matched with the rate of production of alkyl radicals and that excess photoredox might generate radicals faster than they can be

captured by the Ni intermediate, leading to lower AY. It should be noted that the traditional reductants, such as Zn, Mn, TDAE [tetrakis(dimethylamino)ethylene] or B_2Pin_2, only render trace cross-coupling products (Table 1, entries 13–16). This observation suggests a clear advantage of HEH as the reductant, in addition to its increased sustainability over reducing metals. We also tried different aryl electrophiles, and founded that the aryl bromide is the best aryl electrophile in this reaction (see the Supporting Information table S8 for details).

Control experiments further demonstrated that each of 4CzIPN, light, $NiBr_2$·DME and HEH were all essential components for this catalytic system (Table 1, entry 17, one component left out each run). Taken together, our optimized condition for this transformation are: diethyl vinylphosphonate **1a** (0.1 mmol), 1-(4-bromophenyl)ethan-1-one **2a** (0.2 mmol) and 2-bromo-2-methylpropane **3a** (0.4 mmol), HEH (2.0 equiv.), Cy_2NMe (3.0 equiv.), 4CzIPN (1 mol%), $NiBr_2$·DME (10 mol%) and **L1*** (11 mol%) in THF (0.05 mol/L) under blue LED irradiation at room temperature for 24 h (Table 1, entry 12).

Table 1: Optimization of reaction conditions[a]

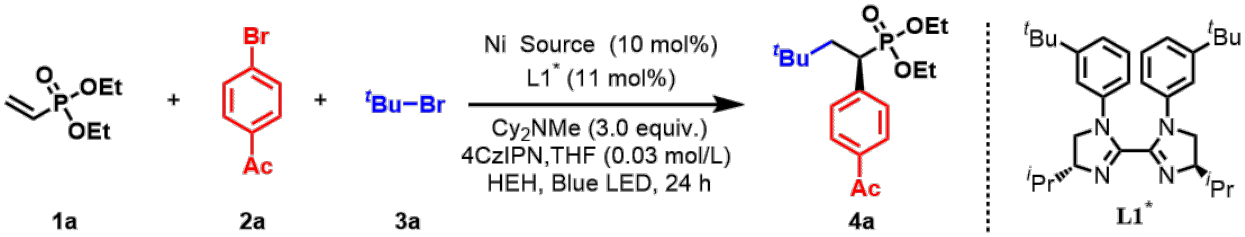

1a 2a 3a 4a L1*

Entry	Ni Source	Solvent	Reductant (equiv.)	4CzIPN (mol%)	AY (%)[b]	Ee (%)[c]
1	$Ni(COD)_2$	DMA	HEH (3 equiv.)	10	25	95
2	$NiBr_2$	DMA	HEH (3 equiv.)	10	48	93
3	NiI_2	DMA	HEH (3 equiv.)	10	54	91
4	$NiBr_2$·DME	DMA	HEH (3 equiv.)	10	60	95
5	$NiBr_2$·DME	DME	HEH (3 equiv.)	10	42	89
6	$NiBr_2$·DME	CPME	HEH (3 equiv.)	10	56	90
7	$NiBr_2$·DME	THF	HEH (3 equiv.)	10	65	95
8	$NiBr_2$·DME	THF	HEH (2 equiv.)	10	73	95
9[d]	$NiBr_2$·DME	THF	HEH (2 equiv.)	10	75	95
10[d]	$NiBr_2$·DME	THF	HEH (2 equiv.)	5	69	95
11[d]	$NiBr_2$·DME	THF	HEH (2 equiv.)	2	63	95
12[d]	$NiBr_2$·DME	THF	HEH (2 equiv.)	1	88 (85)[e]	95
13[d]	$NiBr_2$·DME	THF	Zn (2 equiv.)	1	Trace	ND
14[d]	$NiBr_2$·DME	THF	Mn (2 equiv.)	1	Trace	ND
15[d]	$NiBr_2$·DME	THF	TDAE (2 equiv.)	1	Trace	ND
16[d,f]	$NiBr_2$·DME	THF	B_2Pin_2 (2 equiv.)	1	Trace	ND
17[d]	Without 4CzIPN/blue light/$NiBr_2$·DME/HEH				Trace	ND

[a]All of the experiments were performed with **1a** (0.1 mmol), **2a** (0.2 mmol), **3a** (0.4 mmol) under argon for 24 h.
[b]Assay yield (AY) determined by GC using tetradecane as an internal standard.
[c]Ee was determined by chiral-phase HPLC on a CHIRALPAK IC column.
[d]0.05 mol/L THF was used. Trace: yield <5%. ND: ee was not determined.
[e]Isolated yield.
[f]NaOMe (2 equiv.) was used as the base.

We next investigated the substrate scope of the aryl bromide coupling partners. A wide range of aryl bromides with functional groups at different positions all reacted efficiently with diethyl vinylphosphonate **1a** and 2-bromo-2-methylpropane **3a** with excellent ee values (Scheme 3). As noted, the parent 1-(4-bromophenyl)ethan-1-one **2a** generated the reductive cross-coupling product **4a** with 95% ee (85% isolated yield). Aryl bromides with neutral, electron-donating and electron-withdrawing groups at the 4-position, such as 4-H, 4-^{t}Bu, 4-F, 4-Cl, 4-CF_3, all exhibited high ee values (85%–95%) and moderate to good yields (56%–75%). 4-SMe was also a suitable substituent for this reaction, generating **4g** with 76% yield and 93% ee. Notably, functionalized aryl bromides bearing aldehyde (**2h**), ester (**2i, 2j**), cyano (**2k**), ketone (**2l**) and boronic acid ester (**2m**) also coupled effectively with **1a** and **3a** to render **4h–4m** with 88%–95% ee (52%–81% yield). These results demonstrated that aryl bromides substrates that are susceptible to reduction are not noticeably impacted under the mild reaction conditions. Aryl bromides bearing an acetal (**2n**) or ketone (**2o**) in the 3-position yielded the corresponding products **4n** (60% yield, 95% ee) and **4o** (74% yield, 91% ee). Disubstituted aryl bromides generated products **4p** (53% yield, 93% ee) and **4q** (66% yield, 85% ee).

Heterocyclic compounds are important structural motifs in medicinal chemistry. We found that several heteroaryl bromides, including oxyheteroaryl bromides (**2r–2v**), azaaryl bromides (**2w, 2x**) and 5-bromobenzo[b]thiophene **2y** provided the target products with 85%–96% ee and 51%–92% yields. We further showed that ibuprofen and geraniol derivatives can act as coupling partners and generate the cross-coupling products **4z** (86% de) and **4aa** (89% ee), highlighting the potential utility of this 3-component reaction in late-stage functionalizations. Although the yield of the geraniol product is diminished, it is remarkable that good selectivity for the vinyl phosphonate was observed over the other two double bonds.

To further demonstrate the applications of this 3-component enantioselective cross-electrophile coupling reaction, we tested the reactivity of unactivated alkyl halides **3**. Compared to 2-bromo-2-methylpropane **3a**, 2-bromo-2,6-dimethylheptane **3b** proved effective, providing product **5a** with 94% ee (52% yield). Cyclic tertiary alkyl bromides such as 1-bromo-4-(*tert*-butyl)-1-methylcyclohexane **3c** generated **5b** at a 57% yield with 92% ee. Alkyl bromides with phenyl groups could offer **5c** (51% yield, 92% ee) and **5d** (40% yield, 93% ee), respectively. Tertiary alkyl bromides that contain ester groups were compatible with our standard conditions, providing the cross-coupling products **5e**–**5h** in 52%–83% yield with 94%–96% ee (**5e**, **5g**, **5h**) or 93% de (**5f**). In addition, both cyclic and acyclic secondary alkyl bromides **3j–3o** provided the target product **5i–5n** in 91%–95% ee (44%–65% yield).

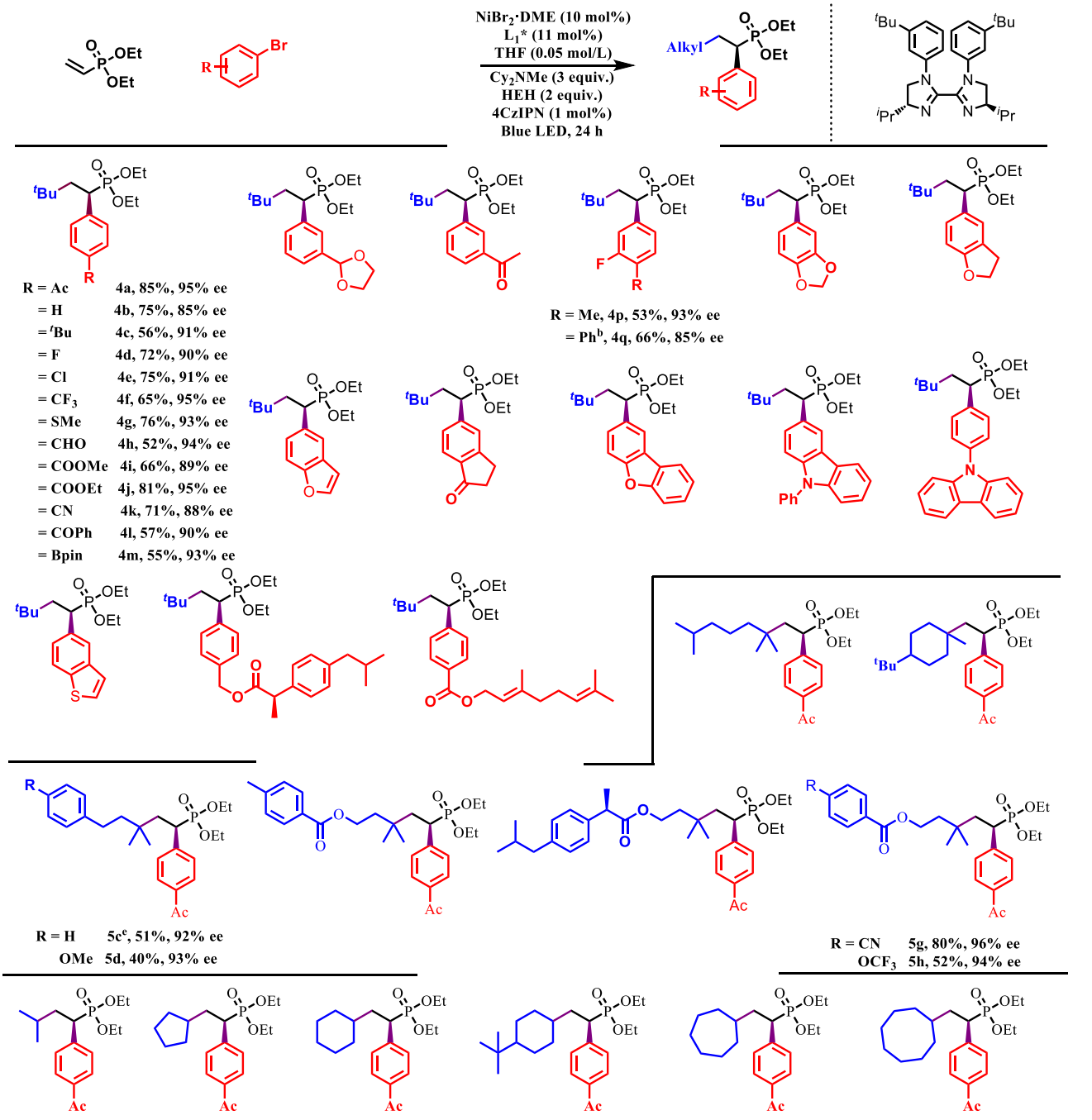

Scheme 3. Substrate scope for enantioselective domino alkyl arylation of vinyl phosphonates

[a]All of the experiments were performed with **1a** (0.1 mmol), **2** (0.2 mmol), **3** (0.4 mmol) under argon atmosphere for 24 h.
[b]$Ni(acac)_2$ (10 mol%) was used.
[c]$Ni(acac)_2$ (20 mol%) and 2-MeTHF (2 mL) were used.
[d]$Ni(acac)_2$ (10 mol%) and THF:2-Me THF=3:1 were used.
[e]$Ni(acac)_2$ (10 mol%) and L1* (15 mol%) were used.
[f]$Ni(ClO_4)_2·6H_2O$ (10 mol%) and THF:2-Me THF = 3:1 were used.
[g]Alkyl iodides instead of alkyl bromides.
[h]$NiCl_2$·DME (10 mol%) and THF:2-MeTHF = 3:1 were used.

Several control experiments were performed to identify the dominant reaction pathway in this tandem process. First, to explore the possible involvement of radical intermediates, we added radical scavenger TEMPO to the standard conditions. TEMPO effectively inhibited the generation of **4a** and the TEMPO-adduct was detected *via* HRMS analysis (Scheme 4a), suggesting the reaction likely proceeds through a radical pathway.

To further probe the generation of *tert*-butyl radicals, we carried out additional control experiments (Scheme 4b). We found that the radical addition/HAT quenching product **6a** was generated in a 68% isolated yield when the standard reaction was conducted in the absence of the Ni catalyst. This indicates that the photoredox catalyst can promote SET with *tert*-butyl bromide to generate the *tert*-butyl radical. To understand whether *tert*-butyl radical formation can occur with the Ni catalysts, diethyl vinylphosphonate **1a** and 2-bromo-2-methylpropane **3a** were subjected to 1.0 equiv. $Ni(COD)_2$/**L1*** catalyst precursors without the photoredox catalyst or blue LED light at room temperature for 24 h. The formation of **6a** at a 23% isolated yield suggests that the nickel catalyst can also trigger the generation of *tert*-butyl radical *via* an SET process. These experiments reveal that both the photoredox catalyst and Ni catalyst can cause the generation of *tert*-butyl radicals.

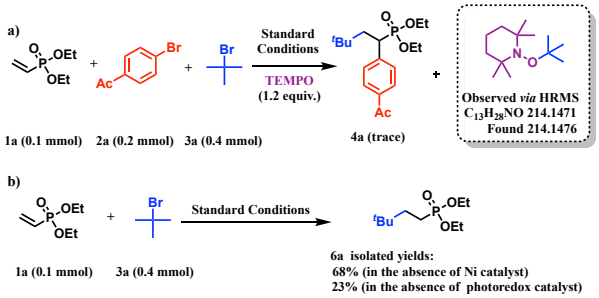

Scheme 4. Radical probe experiments

At the outset, we wondered whether the photoredox catalyst could influence the enantiodetermining step. To study this, we evaluated the reaction with 1.0 equiv. $Ni(COD)_2$ and 1.1 equiv. **L1*** as stoichiometric mediator in the absence of 4CzIPN, HEH and Cy_2NMe. In the event, **4a** was obtained in 26% isolated yield and 95% ee under blue light. In addition, the target product **4a** could be isolated with 22% yield and 95% ee in the dark (Scheme 5a). These ee values in the stoichiometric reactions are consistent with those under the standard catalytic conditions, suggesting that the enantiodetermining step depends on the Ni/**L1*** catalyst precursor and not on the photoredox components or light (Table 1, entry 12).

Next, stepwise experiments were performed to identify which substrate preferentially reacts with **L1***Ni^0 in the catalytic cycle. First, aryl bromide **2a** with a stoichiometric amount of $Ni(COD)_2$ and **L1*** were combined for 30 min, followed by the addition of 1 equiv. of diethyl vinylphosphonate **1a** and 4 equiv. of 2-bromo-2-methylpropane **3a** under otherwise standard conditions. This reaction yielded **4a** in 30% yield with 95% ee (Scheme 5b). It is noteworthy that the ee value is similar to the reaction carried out under the standard catalytic conditions. On the contrary, reaction with alkyl bromide first followed by vinylphosphonate and aryl bromide rendered only trace cross-coupling products (< 5% yield, Scheme 5c). Taken together, these results suggested that the transformation is initiated by the oxidative addition with aryl bromides, rather than alkyl bromides. This result is consistent with the work of Diao and coworkers [43, 79-81].

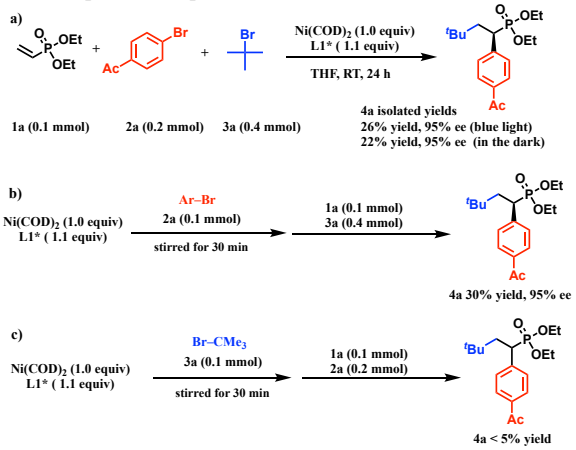

Scheme 5. Probing the enantiodetermining step and stepwise reactions

To define the main roles of HEH and Cy_2NMe, a more detailed product analysis of this three-component enantioselective reductive cross-electrophile coupling reaction was performed, following on our previous studies [57, 70] (Scheme 6). As noted, the target product **4a** was provided in 85% yield and 95% ee under the standard conditions. In the process 1) the HEH was converted into the expected pyridine derivative (**7**, 100% yield); 2) the $Cy_2NMe{\cdot}HBr$ (**8**) was isolated with 72% yield, and 3) the demethylated amine Cy_2NH (**9**) was formed 14% yield. These results indicate that: 1) HEH is the main terminal reductant, 2) Cy_2NMe is primarily the base that neutralizes byproduct HBr, and 3) the Cy_2NMe oxidation with the photoexcited 4CzIPN* to provide the amine radical cation, which then loses H• to generate the iminium ion and undergoes hydrolysis by advantageous water during the reaction or upon workup [82]. Furthermore, lower yields were obtained when Cy_2NMe was replaced by inorganic bases, such as Cs_2CO_3 or Na_2CO_3. These results indicate that both HEH and Cy_2NMe play independent, yet important roles in the overall transformation.

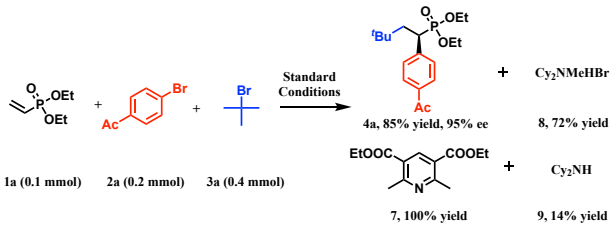

base	*yield (%)*	*ee (%)*
Cs_2CO_3	*0*	*0*
Na_2CO_3	*27*	*93*

Scheme 6. The role of HEH and Cy_2NMe analysis

To further probe the role of HEH in our reaction system, we measured UV/vis absorption spectrum of various combinations of **1a**, **2a**, **3a**, Cy_2NMe and HEH in THF at 0.1 mol/L concentration (Scheme 7a). It is known that the combination of electron-rich HEH with electron-poor

substrates can lead to the formation of electron donor–acceptor (EDA) complexes *via* a π–π interaction [83-87]. UV/vis spectroscopy confirmed the absence of EDA complexes during the reaction, suggesting that HEH cannot induce radicals in our reaction system.

Next, Stern–Volmer quenching experiments were performed with HEH, **1a, 2a, 3a,** Cy_2NMe and **L1***$NiBr_2$ to see which species would quench the reactive [4CzIPN]* (see the Supporting Information for details). Preliminary studies showed that the excited-state [4CzIPN]* was dramatically diminished by 10^{-4} ~ 10^{-3} mol/L of HEH in THF (Scheme 7b). However, **1a, 2a** and **3a** did not lead to detectable quenching effects. It should be noted that Cy_2NMe and **L1***$Ni^{II}Br_2$ had a small effect on the quenching of photocatalyst. These studies indicate that HEH is the main species that quenches the excited-state of [4CzIPN]*. This result is consistent with the role of HEH in Scheme 6.

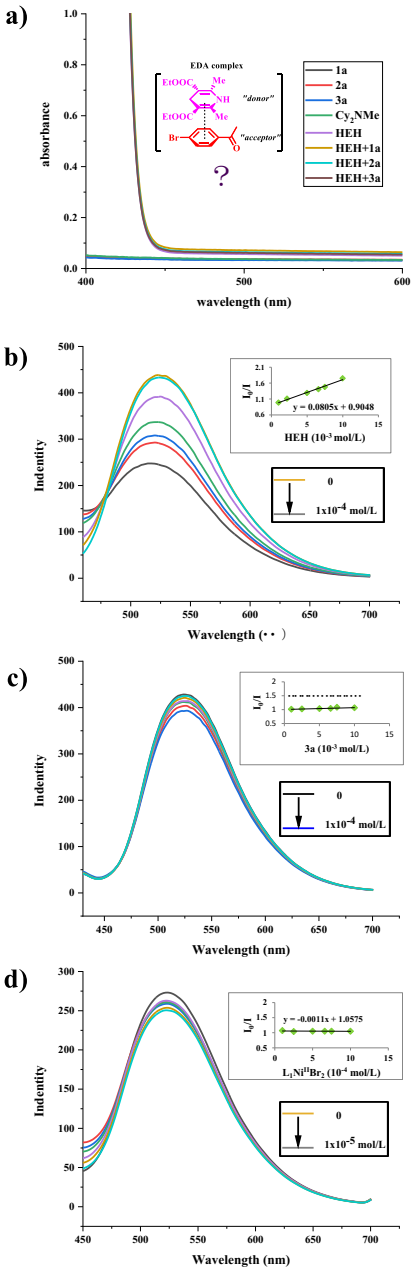

Scheme 7. UV/vis absorption and luminescence quenching experiments

Based on the above-mentioned experiments and previous reports [88], we proposed a possible dual catalytic reaction mechanism in Scheme 8. The active **L1***Ni^0 catalyst precursor **A** [$E1/2^{red}$ (Ni^{II}/Ni^0) = − 1.2 V *vs.* SCE] is formed by the reduced photocatalyst $4CzIPN^{\bullet-}$ ($E1/2^{red}$ = − 1.21 V *vs.* SCE) [89-92] *in situ* in two SET steps, then underwent oxidative addition with aryl bromide to form the **s**quare planar singlet Ni^{II} species ^{1}**C**, which then could undergo spin crossover to give a triplet tetrahedral species ^{3}**C** prior to oxidative capture with the alkyl radical **D** to generate the **L1***Ni^{III} intermediate **E-a**, which could bind the Lewis basic oxygen of the phosphonate. The aryl and bromine occupied two axial sites of the intermediate **E-a** [54, 59]. Reductive

elimination affords the product **4a**. The resultant **L1***Ni^{I}Br complex **F** abstracts the bromine atom from *tert*-butyl bromide **3a** affording the triplet tetrahedral Ni^{II} complex ^{3}**G** and generating the alkyl radical. Intermediate ^{3}**G** then was reduced to regenerate the **L1***Ni^{0} by SET from 2 equiv of [4CzIPN] and closing the catalytic cycles.

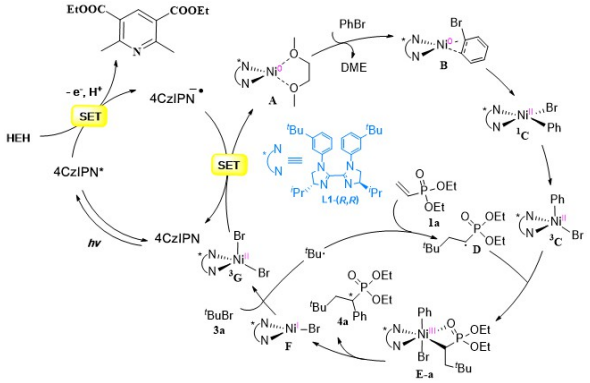

Scheme 8. Proposed catalytic cycles

We wished to gain more insight into the mechanism by elucidating the factors controlling the stereoselectivity, determining the catalyst oxidation state that likely intercepts the radical (Ni^{0} or Ni^{II}) and identifying the enantiodetermining step. Density functional theory (DFT) calculations were, therefore, performed. To reduce the computational cost, phenyl bromide was used. As shown in Scheme 9a, after coordination of the phenyl bromide to the Ni(0) catalyst, the resulting complex **B** can undergo fast oxidative addition (barrier of only 1.8 kcal/mol) to form a square planar singlet **L1***Ni(Br)Ph species ^{1}**C**. Intermediate ^{1}**C** can undergo spin crossover to give a triplet tetrahedral Ni(II) species ^{3}**C** that is 7.5 kcal/mol downhill in energy with respect to ^{1}**C**. Next, ^{3}**C** can oxidatively capture the alkyl radical **D** to form a Ni(III) intermediate (*R*)-**E-a** with a free energy barrier of 8.2 kcal/mol. This 6-coordinate intermediate features a coordinated oxygen of the P=O bond. Subsequently, (*R*)-**E-a** undergoes C–C reductive elimination with a free energy barrier of 14.2 kcal/mol to generate a Ni(I) complex (*R*)-**F**, which then can undergo bromine abstraction with the *tert*-butyl bromide **3a** to afford the triplet tetrahedral Ni(II) complex **L1***NiBr$_2$, (*R*)-^{3}**G** [see Supplementary Figure 3 for geometries and relative energies of (*R*)-^{1}**G** and (*R*)-^{3}**G**] that is downhill in energy by 8.4 kcal/mol with respect to complex (*R*)-**F**.

Other pathways were also explored. For example, it can be envisioned that the Ni(0) species **A** can first react with the *tert*-butyl bromide **3a** (Path-b) or the alkyl radical **D** (Path-c/d). The calculations of Paths-b-d, however, all show that products with *S* configuration would dominant, which is inconsistent with experimental observations. Moreover, the energtic spans [93-94] (also called overall activation energy) of these pathways are all higher than that of Path-a (taking the generation of (*R*)-products as example, for Path-a/b/c/d, ΔG = 14.2, 31.3, 19.1 and 19.1 kcal/mol, respectively, see Supplementary Figures 4, 5 and 6 in the Supporting Information for full energy diagrams). Therefore, Path-a is the preferred pathway.

Interestingly, from the calculations of Path-a, the radical addition to the tetrahedral Ni(II) **L1***Ni(Br)Ph species *via* **TS$_2$-a** is the enantiodetermining step not the reductive elimination step to form the C–C bond. The energy difference between (*R*)-**TS$_2$-a** and (*S*)-**TS$_2$-a** was found to be 2.4 kcal/mol (equivalent to 97% ee), which is consistent with the experimentally observed enantioselectivity (95% ee for **4a**). To investigate the decisive factor for the enantioselectivity in the radical addition step, IGMH analysis [95] was conducted on the two transition states to probe the interactions between the ^{3}**C** moiety and the entering alkyl radical **D** (Scheme 9b). From the IGMH maps, the main interaction region is between the Ni-Ph phenyl ring and the phosphonate group in (*R*)-**TS$_2$-a** and between the Ni-Ph phenyl ring and the alkyl chain in (*R*)-**TS$_2$-a**. These interactions can be attributed to the P=O···π (Ni–Ph phenyl ring) interaction in (*R*)-**TS$_2$-a** and the C–H···π (Ni–Ph phenyl ring) interaction in (*R*)-**TS$_2$-a**, respectively, revealing the van der Waals interaction between triplet **L1***Ni(Br)Ph (^{3}**C**) and the radical **D** (see Supplementary Figure 7). What's more, the more continuous and larger interaction region in (*R*)-**TS$_2$-a** due to the higher electron density between the Ni–Ph phenyl ring and the phosphonate moiety reveals a stronger interaction and finally leads to a shorter developing Ni---C bond (3.27 Å vs 3.39 Å, as shown in the 3D geometries of (*R*)-**TS$_2$-a** and (*R*)-**TS$_2$-a** in Scheme 9). Overall, the disparity in van der Waals interactions is derived from the different orientation of the phosphonate group in the (*R*)- and (*S*)-conformations, which play an essential role in controlling the enantioselectivity.

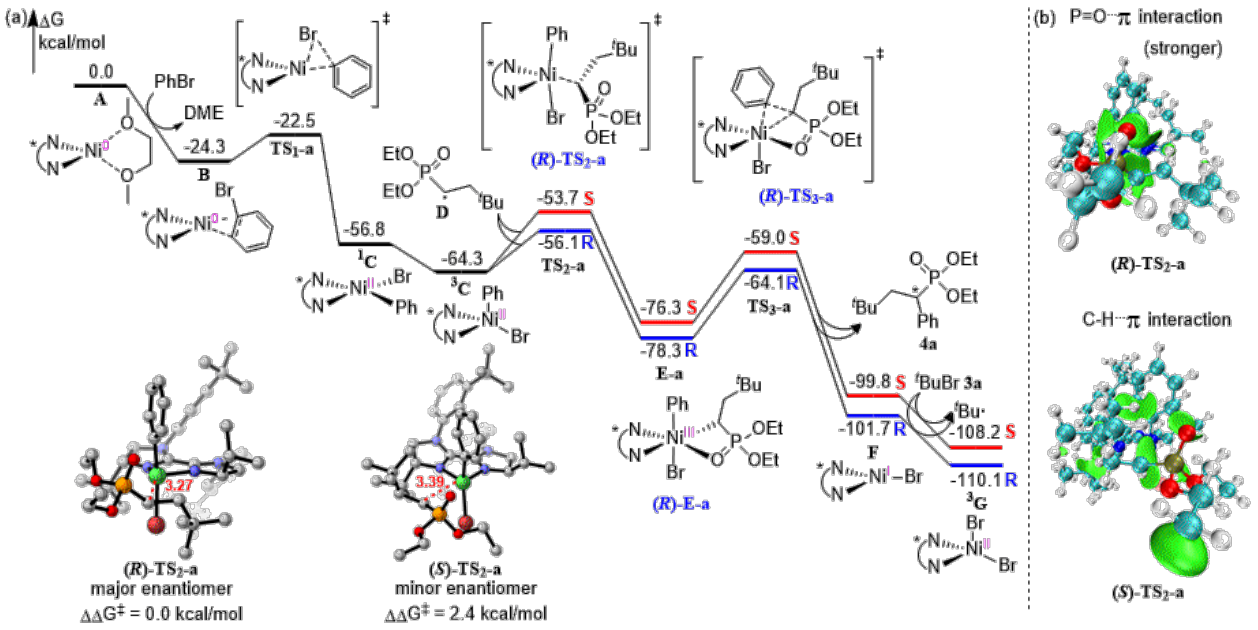

Scheme 9. DFT calculation of Path-a. (a) Relative Gibbs free energy values were computed at the M06L-D3/SDD-6-311+G(d,p)/SMD(THF)//B3LYP-D3(BJ)/SDD-6-31G(d) level of theory. (b) Sign(λ2)ρ colored isosurfaces of δg^{inter} = 0.005 a.u. corresponding to IGMH analyses for (*R*)-TS_2-a and (*S*)-TS_2-a. The intermediate ^{3}C and alkyl radical D are defined as the two fragments.

3. Conclusion

We have described an enantioselective three-component alkyl arylation of vinyl phosphonates with aryl bromides and unactivated alkyl halides *via* a photoredox/nickel-catalyzed cross-electrophile coupling process. This protocol provides a facile way to construct a diverse array of functionalized chiral *α*-aryl phosphonates with high enantioselectivities (up to 96% ee) and good to excellent yields (up to 92%). Moreover, this method avoids the use of preformed brominated phosphorus reagents and organometallic reagents and is free of metal reductants, minimizing the generation of metal waste. Mechanistic studies demonstrate that the **L1***Ni(Ar)Br intercepts the phosphonates stabilized radical. Our results stand in contrast to the seminal findings of Kozlowski and Molander on a $Ni^{0/I/III}$ mechanism, wherein a benzylic radical reversibly adds to the Ni catalyst [96]. These differences demonstrate how small changes manifest themselves in divergent reaction pathways. IGMH analysis in our system revealed that the van der Waals interaction between the phosphonate group phenyl ring (P=O···π interaction) play an essential role in controlling the enantioselectivity. These new findings build a platform for further designing asymmetric three-component cross-electrophile coupling reactions. Related enantioselective reductive cross-electrophile reactions are currently under development in our laboratories.

Declaration of competing interest

The authors declare that they have no known competing financial interests or personal relationships that could have appeared to influence the work reported in this paper.

Acknowledgments

The authors acknowledge the National Natural Science Foundation of China (22071107), Natural Science Foundation of Jiangsu Province, China (BK20211588, BK20220328), Natural Science Research Projects of Colleges and Universities in Jiangsu Province (22KJB150005), Jiangsu Excellent Postdoctoral Program (287706). PJW thanks the US NSF (CHE-2154593).

References

[1] N. Zhang and J. E. Casida, Bioorg. Med. Chem. 10 (2002) 1281-1290.
[2] D. Wu, J.-Q. Niu, Y.-H. Ding, X.-Y. Wu, B.-H. Zhong and X.-W. Feng, Med. Chem. Res. 21 (2012) 1179-1187.
[3] E. R. Jackson and C. S. Dowd, Curr. Top. Med. Chem. 12 (2012) 706-728.
[4] S. Montel, C. Midrier, J.-N. Volle, R. Braun, K. Haaf, L. Willms, J.-L. Pirat and D. Virieux, Eur. J. Org. Chem. 2012 (2012) 3237-3248.
[5] S. Wendels, T. Chavez, M. Bonnet, K. A. Salmeia and S. Gaan, Materials 10 (2017) 784/781-784/732.
[6] J. M. Lipshultz, G. Li and A. T. Radosevich, J. Am. Chem. Soc. 143 (2021) 1699-1721.
[7] W. Tang and X. Zhang, Chem. Rev. 103 (2003) 3029-3069.
[8] P. W. N. M. van Leeuwen, P. C. J. Kamer, C. Claver, O. Pamies and M. Dieguez, Chem. Rev. 111 (2011) 2077-2118.
[9] J. A. Bisceglia and L. R. Orelli, Curr. Org. Chem. 16 (2012) 2206-2230.
[10] C. Queffelec, M. Petit, P. Janvier, D. A. Knight and B. Bujoli, Chem. Rev. 112 (2012) 3777-3807.
[11] J.-J. Feng, X.-F. Chen, M. Shi and W.-L. Duan, J. Am. Chem. Soc. 132 (2010) 5562-5563.

[12] J. Lu, J. Ye and W.-L. Duan, Org. Lett. 15 (2013) 5016-5019.
[13] M. Hatano, T. Horibe and K. Ishihara, Angew. Chem., Int. Ed. 52 (2013) 4549-4553.
[14] Z. Lu, H. Zhang, Z. Yang, N. Ding, L. Meng and J. Wang, ACS Catal. 9 (2019) 1457-1463.
[15] W.-J. Yue, J.-Z. Xiao, S. Zhang and L. Yin, Angew. Chem., Int. Ed. 59 (2020) 7057-7062.
[16] Y. He, C. Liu, L. Yu and S. Zhu, Angew. Chem., Int. Ed. 59 (2020) 9186-9191.
[17] K. Dong, Z. Wang and K. Ding, J. Am. Chem. Soc. 134 (2012) 12474-12477.
[18] S. E. Denmark and C.-T. Chen, J. Am. Chem. Soc. 117 (1995) 11879-11897.
[19] L. Bernardi, W. Zhuang and K. A. Jorgensen, J. Am. Chem. Soc. 127 (2005) 5772-5773.
[20] L. Bernardi and K. A. Jorgensen, Chem. Commun. (2005) 1324-1326.
[21] F. Palacios, C. Alonso and J. M. De los Santos, Chem. Rev. 105 (2005) 899-931.
[22] N. A. Strotman, S. Sommer and G. C. Fu, Angew. Chem., Int. Ed. 46 (2007) 3556-3558.
[23] N. Rabasso and A. Fadel, Tetrahedron Lett. 55 (2014) 6068-6071.
[24] S.-J. He, J.-W. Wang, Y. Li, Z.-Y. Xu, X.-X. Wang, X. Lu and Y. Fu, J. Am. Chem. Soc. 142 (2020) 214-221.
[25] S. Montel, L. Raffier, Y. He and P. J. Walsh, Org. Lett. 16 (2014) 1446-1449.
[26] S. Montel, T. Jia and P. J. Walsh, Org. Lett. 16 (2014) 130-133.
[27] Y. Liang and G. C. Fu, J. Am. Chem. Soc. 137 (2015) 9523-9526.
[28] J. Schmidt, J. Choi, A. T. Liu, M. Slusarczyk and G. C. Fu, Science 354 (2016) 1265-1269.
[29] H. Huo, B. J. Gorsline and G. C. Fu, Science 367 (2020) 559-564.
[30] Y. Zhao and D. J. Weix, J. Am. Chem. Soc. 137 (2015) 3237-3240.
[31] L. K. G. Ackerman, M. M. Lovell and D. J. Weix, Nature 524 (2015) 454-457.
[32] E. C. Hansen, D. J. Pedro, A. C. Wotal, N. J. Gower, J. D. Nelson, S. Caron and D. J. Weix, Nat. Chem. 8 (2016) 1126-1130.
[33] A. H. Cherney, N. T. Kadunce and S. E. Reisman, J. Am. Chem. Soc. 135 (2013) 7442-7445.
[34] J. L. Hofstra, A. H. Cherney, C. M. Ordner and S. E. Reisman, J. Am. Chem. Soc. 140 (2018) 139-142.
[35] K. E. Poremba, S. E. Dibrell and S. E. Reisman, ACS Catal. 10 (2020) 8237-8246.
[36] T. J. DeLano, S. E. Dibrell, C. R. Lacker, A. R. Pancoast, K. E. Poremba, L. Cleary, M. S. Sigman and S. E. Reisman, Chem. Sci. 12 (2021) 7758-7762.
[37] B. P. Woods, M. Orlandi, C.-Y. Huang, M. S. Sigman and A. G. Doyle, J. Am. Chem. Soc. 139 (2017) 5688-5691.
[38] E. E. Stache, T. Rovis and A. G. Doyle, Angew. Chem., Int. Ed. 56 (2017) 3679-3683.
[39] S. H. Lau, M. A. Borden, T. J. Steiman, L. S. Wang, M. Parasram and A. G. Doyle, J. Am. Chem. Soc. 143 (2021) 15873-15881.
[40] D. Sun, G. Ma, X. Zhao, C. Lei and H. Gong, Chem. Sci. 12 (2021) 5253-5258.
[41] J. Liu, H. Gong and S. Zhu, Angew. Chem., Int. Ed. 60 (2021) 4060-4064.
[42] D. Anthony, Q. Lin, J. Baudet and T. Diao, Angew. Chem., Int. Ed. 58 (2019) 3198-3202.
[43] J. Diccianni, Q. Lin and T. Diao, Acc. Chem. Res. 53 (2020) 906-919.
[44] Z.-X. Tian, J.-B. Qiao, G.-L. Xu, X. Pang, L. Qi, W.-Y. Ma, Z.-Z. Zhao, J. Duan, Y.-F. Du, P. Su, X.-Y. Liu and X.-Z. Shu, J. Am. Chem. Soc. 141 (2019) 7637-7643.
[45] J.-B. Qiao, Y.-Q. Zhang, Q.-W. Yao, Z.-Z. Zhao, X. Peng and X.-Z. Shu, J. Am. Chem. Soc. 143 (2021) 12961-12967.
[46] W.-Y. Ma, G.-Y. Han, S. Kang, X. Pang, X.-Y. Liu and X.-Z. Shu, J. Am. Chem. Soc. 143 (2021) 15930-15935.
[47] Y. Jin and C. Wang, Angew. Chem., Int. Ed. 58 (2019) 6722-6726.
[48] Y. Lan and C. Wang, Commun. Chem. 3 (2020) 45-53.
[49] Y. Jin, H. Yang and C. Wang, Org. Lett. 22 (2020) 2724-2729.
[50] P. Fan, Y. Lan, C. Zhang and C. Wang, J. Am. Chem. Soc. 142 (2020) 2180-2186.
[51] Z. Lin, Y. Jin, W. Hu and C. Wang, Chem. Sci. 12 (2021) 6712-6718.
[52] T. Lin, J. Mi, L. Song, J. Gan, P. Luo, J. Mao and P. J. Walsh, Org. Lett. 20 (2018) 1191-1194.
[53] H.-Y. Tu, F. Wang, L. Huo, Y. Li, S. Zhu, X. Zhao, H. Li, F.-L. Qing and L. Chu, J. Am. Chem. Soc. 142 (2020) 9604-9611.
[54] L. Guo, M. Yuan, Y. Zhang, F. Wang, S. Zhu, O. Gutierrez and L. Chu, J. Am. Chem. Soc. 142 (2020) 20390-20399.
[55] Y. He, C. Liu, L. Yu and S. Zhu, Angew. Chem., Int. Ed. 59 (2020) 21530-21534.
[56] N. Cui, T. Lin, Y.-E. Wang, J. Wu, Y. Han, X. Xu, F. Xue, D. Xiong, P. J. Walsh and J. Mao, Org. Lett. 24 (2022) 3987-3992.
[57] H. Guan, Q. Zhang, P. J. Walsh and J. Mao, Angew. Chem., Int. Ed. 59 (2020) 5172-5177.
[58] Q. Wang, Y. Qi, X. Gao, L. Gong, R. Wan, W. Lei, Z. Wang, J. Mao, H. Guan, W. Li and P. J. Walsh, Green Synthesis and Catalysis 4 (2023) 89-103.
[59] H. Wang, P. Zheng, X. Wu, Y. Li and T. Xu, J. Am. Chem. Soc. 144 (2022) 3989-3997.
[60] M. Parasram, B. J. Shields, O. Ahmad, T. Knauber and A. G. Doyle, ACS Catal. 10 (2020) 5821-5827.
[61] T. J. Steiman, J. Liu, A. Mengiste and A. G. Doyle, J. Am. Chem. Soc. 142 (2020) 7598-7605.
[62] P. Zheng, P. Zhou, D. Wang, W. Xu, H. Wang and T. Xu, Nat. Commun. 12 (2021) 1646.
[63] W. Xu, P. Zheng, J. Zhou, Z. Hu and T. Xu, Angew. Chem., Int. Ed. 61 (2022) e202214213.
[64] P. Zheng, W. Xu, H. Wang, D. Wang, X. Wu and T. Xu, ACS Catal. 12 (2022) 14926-14933.
[65] J. Zhou, D. Wang, W. Xu, Z. Hu and X. U. Tao, J. Am. Chem. Soc. 145 (2023) 2081-2087.
[66] H. Wang, X. Wu and T. Xu, Angew. Chem., Int. Ed. 62 (2023) e202218299.
[67] S. Dongbang and A. G. Doyle, J. Am. Chem. Soc. 144 (2022) 20067-20077.
[68] S. Zhu, X. Zhao, H. Li and L. Chu, Chem. Soc. Rev. 50 (2021) 10836-10856.
[69] X. Wei, W. Shu, A. Garcia-Dominguez, E. Merino and C. Nevado, J. Am. Chem. Soc. 142 (2020) 13515-13522.
[70] P. Qian, H. Guan, Y.-E. Wang, Q. Lu, F. Zhang, D. Xiong, P. J. Walsh and J. Mao, Nat. Commun. 12 (2021) 6613-6621.

[71] Q. Lu, H. Guan, Y.-E. Wang, D. Xiong, T. Lin, F. Xue and J. Mao, J. Org. Chem. 87 (2022) 8048-8058.
[72] X. Feng, L. Guo, S. Zhu and L. Chu, Synlett 32 (2021) 1519-1524.
[73] X. Li, M. Yuan, F. Chen, Z. Huang, F.-L. Qing, O. Gutierrez and L. Chu, Chem 9 (2023) 154-169.
[74] A. Garcia-Dominguez, R. Mondal and C. Nevado, Angew. Chem., Int. Ed. 58 (2019) 12286-12290.
[75] S.-Z. Sun, Y. Duan, R. S. Mega, R. J. Somerville and R. Martin, Angew. Chem., Int. Ed. 59 (2020) 4370-4374.
[76] C. Zhu, H. Yue, B. Maity, I. Atodiresei, L. Cavallo and M. Rueping, Nat. Catal. 2 (2019) 678-687.
[77] H. Yue, C. Zhu, R. Kancherla, F. Liu and M. Rueping, Angew. Chem., Int. Ed. 59 (2020) 5738-5746.
[78] T. Lin, Y.-E. Wang, N. Cui, M. Li, R. Wang, J. Bai, Y. Fan, D. Xiong, F. Xue, P. J. Walsh and J. Mao, J. Org. Chem. 87 (2022) 16567-16577.
[79] Q. Lin, Y. Fu, P. Liu and T. Diao, J. Am. Chem. Soc. 143 (2021) 14196-14206.
[80] J. B. Diccianni and T. Diao, Trends Chem. 1 (2019) 830-844.
[81] Q. Lin, E. H. Spielvogel and T. Diao, Chem 9 (2023) 1295-1308.
[82] X. Fan, X. Gong, M. Ma, R. Wang and P. J. Walsh, Nat. Commun. 9 (2018) 1-8.
[83] B. Liu, C.-H. Lim and G. M. Miyake, J. Am. Chem. Soc. 139 (2017) 13616-13619.
[84] J. Wu, P. S. Grant, X. Li, A. Noble and V. K. Aggarwal, Angew. Chem., Int. Ed. 58 (2019) 5697-5701.
[85] G. E. M. Crisenza, D. Mazzarella and P. Melchiorre, J. Am. Chem. Soc. 142 (2020) 5461-5476.
[86] L. M. Kammer, S. O. Badir, R.-M. Hu and G. A. Molander, Chem. Sci. 12 (2021) 5450-5457.
[87] T. Yang, Y. Wei and M. J. Koh, ACS Catal. 11 (2021) 6519-6525.
[88] M. Neumann, S. Fueldner, B. Koenig and K. Zeitler, Angew. Chem., Int. Ed. 50 (2011) 951-954.
[89] J. C. Tellis, D. N. Primer and G. A. Molander, Science 345 (2014) 433-436.
[90] Z. Zuo, D. T. Ahneman, L. Chu, J. A. Terrett, A. G. Doyle and D. W. C. MacMillan, Science 345 (2014) 437-440.
[91] Z. Zuo, H. Cong, W. Li, J. Choi, G. C. Fu and D. W. C. MacMillan, J. Am. Chem. Soc. 138 (2016) 1832-1835.
[92] Q.-Y. Meng, S. Wang, G. S. Huff and B. Koenig, J. Am. Chem. Soc. 140 (2018) 3198-3201.
[93] S. Kozuch and S. Shaik, Acc. Chem. Res. 44 (2011) 101-110.
[94] S. Kozuch and S. Shaik, J. Am. Chem. Soc. 128 (2006) 3355-3365.
[95] T. Lu and Q. Chen, J. Comput. Chem. 43 (2022) 539-555.
[96] O. Gutierrez, J. C. Tellis, D. N. Primer, G. A. Molander and M. C. Kozlowski, J. Am. Chem. Soc. 137 (2015) 4896-4899.